Effect of electrical stimulation on biological cells by capacitive coupling – an efficient numerical study considering model uncertainties

Julius Zimmermann, Richard Altenkirch, and Ursula van Rienen, *Member, IEEE*

***Abstract*— Electrical stimulation of biological samples such as tissues and cell cultures attracts growing attention due to its capability of enhancing cell activity, proliferation and differentiation. Eventually, profound knowledge of the underlying mechanisms paves the way for innovative therapeutic devices. Capacitive coupling is one option of delivering electric fields to biological samples and has advantages with regard to biocompatibility. However, the mechanism of interaction is not well understood. Experimental findings could be related to voltage-gated channels, which are triggered by changes of the transmembrane potential (TMP). Numerical simulations by the Finite Element method (FEM) provide a possibility to estimate the TMP. For realistic simulations of *in vitro* electric stimulation experiments, a bridge from the mesoscopic level down to the cellular level has to be found. A special challenge poses the ratio between the cell membrane (a few nm) and the general setup (some cm). Hence, a full discretization of the cell membrane becomes prohibitively expensive for 3D simulations. We suggest using an approximate FE method that makes 3D multi-scale simulations possible. Starting from an established 2D model, the chosen method is characterized and applied to realistic *in vitro* situations. A to date not investigated parameter dependency is included and tackled by means of Uncertainty Quantification (UQ) techniques. It reveals a strong, frequency-dependent influence of uncertain parameters on the modeling result.**

***Index Terms*— Approximation methods, Bioelectric phenomena, Cellular biophysics, Computational biophysics, Computational electromagnetics, Finite element analysis, Uncertainty Quantification, Tissue engineering**

I. Introduction

In the field of tissue engineering and regenerative medicine researchers are in quest of new therapeutic approaches. One approach is electric stimulation (ES) of biological samples and tissue [1]–[11]. A biological sample could be a piece of human-derived tissue or cells in a particular environment (culture medium, scaffold). The scope of the stimulation is varied. In the field of tissue engineering there are two main goals. On the one hand, the differentiation of stem cells shall be guided by ES. On the other hand, the regeneration of the extracellular matrix by enhanced protein expression of the stimulated cells is desired. There are three different experimental ES approaches [10], [11]

1) direct contact,
2) capacitive coupling,
3) semi-capacitive coupling.

They are distinguishable by the interaction of the electrodes and the biological sample as well as the electric signal that generates the stimulating electric field. In the case of direct contact, the electrodes are in immediate contact with the biological sample. This may imply changes of the sample by, for example, chemical reactions at the electrode, which alter the samples configuration. On the other hand, capacitive coupling remedies this drawback by isolating the electrodes from the sample. The electrodes may for instance be placed outside a Petri dish that contains the sample [12]. Semi-capacitive coupling refers to the case, where one electrode is in contact and the other one is isolated from the sample. For direct contact experiments, often direct current (DC) signals [13] or low-frequency waves are used [14]. In contrast, capacitive coupling requires higher frequencies to induce electric fields through the insulating material [15]–[17].

Experimental studies have been conducted on the mechanism of interaction between the electric field and the cells. Two dominant pathways have been determined. They involve

1) voltage-gated channels [10], [18], [19], which are triggered by changes of the transmembrane potential (TMP) of about $100\,\mathrm{mV}$ [10]. Other studies assume a change of the TMP by $1\,\mathrm{mV}$ to be sufficient [20].
2) stretch-activated channels [10], [21], which may be activated by electroconformation or redistribution [21].

By means of the Finite Element method (FEM), both the electric potential and field in ES experiments can be numerically computed. *In vitro* experiments can be translated into numerical models by taking into account the geometrical dimensions as well as material parameters [22]. Usually, only the electric field on the mesoscopic scale, for example, the field distribution in the Petri dish, is determined for ES experiments. To enable conclusions on the mechanism of interaction, the stimulated cells have to be considered as well. Due to the high aspect ratio between cell membrane and the general

This research was supported by the German Research Foundation (Deutsche Forschungsgemeinschaft, DFG) within the Collaborative Research Center 1270 ELAINE.

Julius Zimmermann and Ursula van Rienen are with the Institute of General Electrical Engineering, University of Rostock, D-18059 Rostock, Germany (email: julius.zimmermann@uni-rostock.de, ursula.van-rienen@uni-rostock.de).

Richard Altenkirch is with the Institute of Physics, University of Rostock, D-18059 Rostock, Germany (email: richard.altenkirch@uni-rostock.de).

Ursula van Rienen is with the Department Life, Light & Matter, University of Rostock, D-18051 Rostock, Germany.

setup, computations discretizing the entire geometry have been mostly carried out for 2D models [17], [23]. However, approximate methods can be used to avoid a discretization of the cell membrane [24], [25]. By employing such methods, simulations of 3D geometries including cells are possible. The TMP is included in the FEM solution and can readily be extracted.

To our knowledge, this approximate method has not yet been used to estimate the effect of capacitively-coupled electric fields on biological cells. In capacitive coupling, the cell membrane might be in direct contact with a good insulator. This is different to the previously studied configurations, where the cell membrane is enclosed by rather conductive cell culture medium. We also consider the uncertainty of the cell's dielectric parameters, which has not been taken into account in previous studies of cells exposed to capacitively-coupled electric fields [17], [23].

In Sec. II, we introduce the numerical method and its approximation. Moreover, we comment on the choice of different material parameters. The approximate method is validated for an established 2D geometry in Sec. III-A.1. In a next step, the influence of the membrane conductivity on the modeling outcome is revealed in Sec. III-A.2. Subsequently, the uncertainties of the input parameters are propagated through the model by a UQ method. In the next section, it is shown how this approach can be used under the consideration of experimental data. Moreover, an outlook on the usability of the presented approach for 3D simulations is given in Sec. III-B.2. The results are discussed in Sec. IV and an conclusion is drawn in Sec. V.

II. Methods and Numerical Model

Electromagnetic fields are in general described by Maxwell's equations. These time-dependent equations can be simplified under certain circumstances. In many therapeutic approaches for biological systems, slowly varying electromagnetic fields can be assumed [26]. In the so called electro-quasistatic regime [27], the electric fields are curl-free and often time-harmonic. Thus, no magnetic field and no eddy currents are present; the displacement current prevails. In this regime, the electric potential Φ for capacitive coupling with time-harmonic input signals can be described by the field equation

$$\nabla \cdot [\sigma^*(\mathbf{r},\omega)\, \nabla\Phi(\mathbf{r})] = 0 \ , \tag{1}$$

where the complex conductivity σ^* equals $\sigma(\mathbf{r},\omega)+j\,\omega\epsilon(\mathbf{r},\omega)$. In this study, the conductivity $\sigma(\mathbf{r},\omega)$ and permittivity $\epsilon(\mathbf{r},\omega)$ are assumed to be constant in the respective subdomains of the model. Moreover, the frequency dependence of the dielectric properties is neglected. This approximation is valid up to about $1\,\mathrm{MHz}$ [28]. From the solution of (1), the electric field can be computed as $\mathbf{E} = -\nabla\Phi$. However, for the processes on the cellular level the TMP is the quantity of interest. It is defined as

$$\mathrm{TMP} = |\Phi_\mathrm{o} - \Phi_\mathrm{i}| \ , \tag{2}$$

where Φ_i is the potential at the inside of the membrane and Φ_o at the outside of the membrane. We also investigated the phase of the TMP as it is a complex number. Here, a change of the sign of the TMP changes the phase by $180°$. We chose the phase to be between $-90°$ and $90°$.

In the conventional FEM approach, the entire geometry is discretized into geometrical elements, for example tetrahedra. To avoid discretizing the membrane with its small thickness d_m, it can be represented by a boundary line that fulfills the condition

$$\mathbf{n}\cdot\mathbf{J}_\mathrm{o,i} = \pm\frac{\sigma^*_\mathrm{m}}{d_\mathrm{m}}\,(\Phi_\mathrm{o}-\Phi_\mathrm{i}) = \mp\frac{\sigma^*_\mathrm{m}}{d_\mathrm{m}}\mathrm{TMP} \tag{3}$$

for the electric current density $\mathbf{J}_\mathrm{o,i}$ on the outside and inside of the membrane, respectively [24]. The complex conductivity of the membrane σ^*_m contains its dielectric properties. As stated in (3), the TMP is already part of this formulation and can be readily accessed. The condition (3) is implemented in commercial software packages such as COMSOL Multiphysics®. In recent years, solutions to similar problems utilizing open-source finite element software have been published [29]–[31]. However, they mostly focus on the time-domain formulation of (1). Thus, they do not utilize complex numbers, which are required to solve the problem described here. Hence, we used COMSOL Multiphysics®, V5.3a to solve (1). All computations were performed on a workstation with 24 physical Intel® Xeon® CPU Gold 6136, $3.00\,\mathrm{GHz}$ cores and $256\,\mathrm{GB}$ RAM.

A first numerical study on the effect of ES on the membrane has been presented by Taghian *et al.* [17]. A 2D domain of $50\,\mu\mathrm{m}$ height and $100\,\mu\mathrm{m}$ width with an abstract cell model has been used (see Fig. 1). Recently, the same model was described in an axisymmetric setting [23]. This assumes a cylindrical Petri dish, wish is a valid choice in many cases. Moreover, the axisymmetric approach mimics true 3D-behavior better than the 2D model presented in [17] as the (hemi-)spherical shape of the cell is accounted for. In contrast, a pure 2D approach assumes the cell to be an infinitely long (hemi-)cylinder. Thus, we focused also on the axisymmetric model and did all our 2D calculations under the assumption of axisymmetry.

In the existing models of a capacitive-coupling setting, the cell membrane has had a thickness of $5\,\mathrm{nm}$ and has been meshed explicitly [17], [23]. We also meshed the membrane explicitly (see Figs. 2 and 3), but in addition described it by (3). Whenever the condition (3) is used, we refer to it as 'contact impedance'. Due to the aspect ratio between the scales, the meshing is a numerically expensive and error-prone task [28]. To obtain an accurate result, we discretized the membrane such that it is represented by at least four layers of triangular elements (see Fig. 2) and even finer where the membrane has a rather sharp edge (see Fig. 3). This yielded $1{,}390{,}530$ DOFs with quadratic Lagrange elements. Note that such a discretization appeared to be impossible in the 3D case on our workstation. In the 'contact impedance' case, the distance of the nodes on the membrane was set to be less than $0.1\,\mu\mathrm{m}$. Also, the edges, where the cell is in contact with the substrate, were refined such that the results converged well. This yielded $31{,}713$ DOFs.

The frequency was varied from $10\,\mathrm{Hz}$ to $100\,\mathrm{MHz}$. In tissue-engineering experiments employing capacitive coupling, frequencies in the range of kHz are used, for example for stim-

ulation of cartilage cell cultures [19], [32], [33] or cartilage explants [12], [34].

The solution was evaluated along the membrane as shown in Fig. 4 and the data exported to ASCII text files. These files were processed by self-written python routines that can be found on github together with the COMSOL Multiphysics®application files [35]. The solution on the two sides of the membrane is accessible for 'contact impedance' calculations by the built-in 'up' and 'down' operators. The corresponding side of the membrane can be determined by plotting the normal vectors in the respective direction (see Fig. 5).

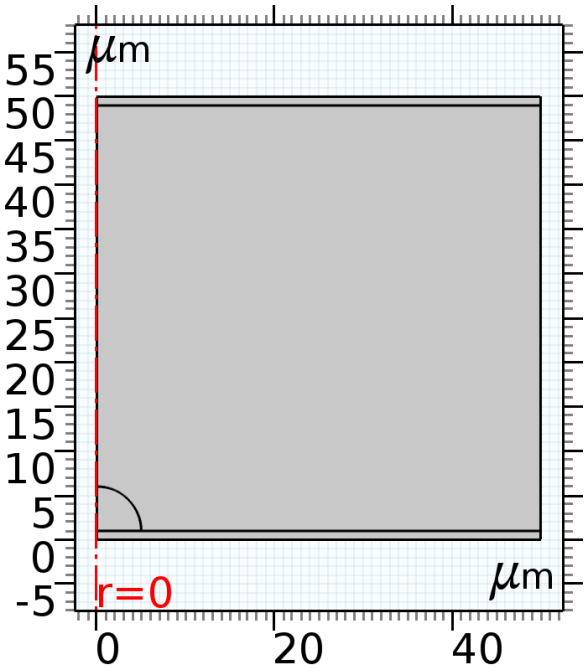

Fig. 1. Axisymmetric model of a cell on a substrate exposed to capacitively-coupled fields [17]. It features two rectangular insulators of thickness $1\,\mu\mathrm{m}$ on top and bottom of the domain, respectively. The cell has a radius of $5\,\mu\mathrm{m}$ and its membrane a thickness of $5\,\mathrm{nm}$. On the top and bottom boundaries of the domain Dirichlet boundary conditions are applied to imply a net voltage difference. The other boundaries are electrically insulating. Material parameters for the cell cytoplasm and the culture medium are assigned as stated in Table I.

TABLE I
PARAMETERS FOR THE NUMERICAL MODEL AS REPORTED IN [17], [23]

Domain	Quantity	Value
Insulator	conductivity	$0\,\mathrm{S/m}$
	rel. permittivity	2.6
Culture medium	conductivity	$1.5\,\mathrm{S/m}$
	rel. permittivity	80
Cytoplasm	conductivity	$1.5\,\mathrm{S/m}$
	rel. permittivity	80
Cell membrane	conductivity	$0\,\mathrm{S/m}$
	rel. permittivity	11.3

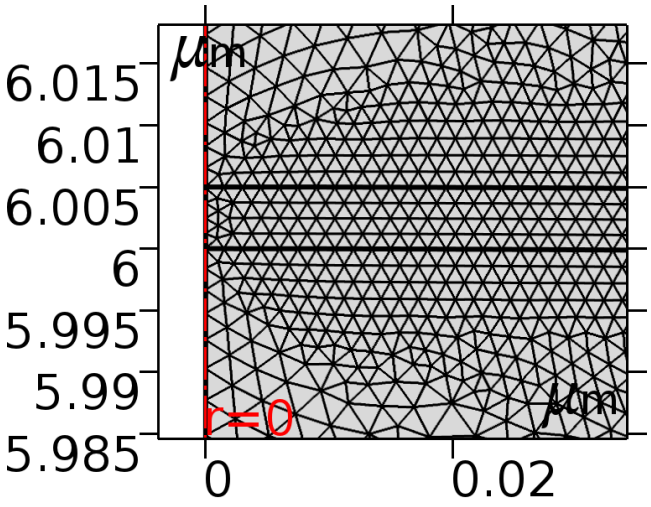

Fig. 2. Discretization of the cell membrane (between 6 and $6.005\,\mu\mathrm{m}$) at the cell's apex. In red, the symmetry axis is shown.

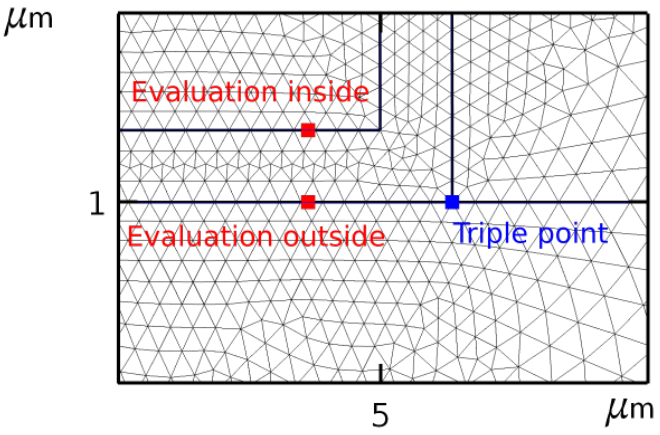

Fig. 3. Discretization of the cell membrane at the cell's right corner close to the triple point. The evaluation along the membrane is presented for one of the evaluation points shown in Fig. 4.

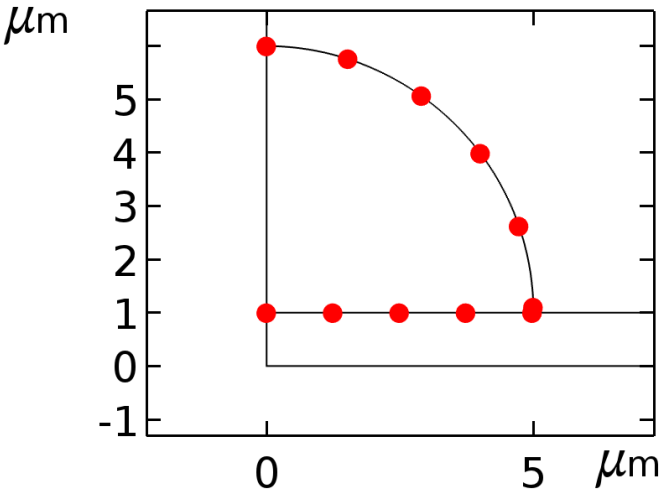

Fig. 4. Points for evaluation of TMP. Note that the triple point is here covered by two points, one on the circular and one on the bottom line part of the cell membrane.

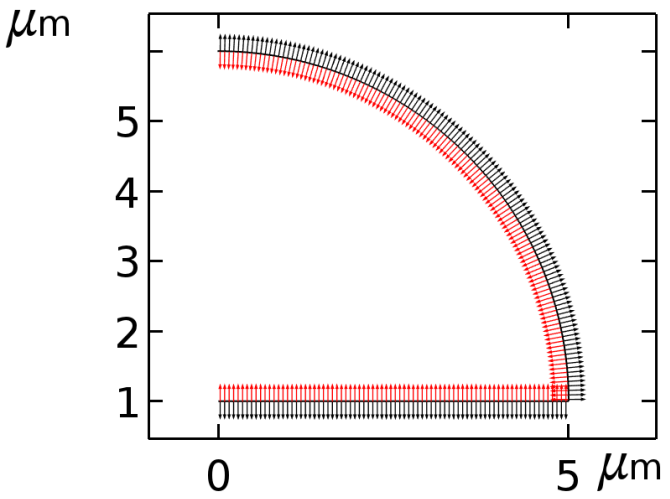

Fig. 5. Normal vectors of the 'down' (black) and 'up' (red) operator on the cell membrane. This means that the operator 'up' accesses the values on the outside of the membrane, i.e. Φ_o and 'down' accesses on the inside, i.e. Φ_i. More information on how to access this information is given online [36].

III. Results

Before applying UQ techniques and allowing for experimentally determined material parameters, we focus on the validation of the numerical approach. The approximate method is compared against the full fidelity model at prominent points along the cell membrane (see Fig. 4). The points at the bottom line of the membrane facing the substrate are characterized by their distance to the center at $x = 0\,\mu\mathrm{m}$. The points on the circular part are characterized by their angle with the vector pointing from $(0\,\mu\mathrm{m}, 0\,\mu\mathrm{m})$ to the apex at $(0\,\mu\mathrm{m}, 5\,\mu\mathrm{m})$. The TMP in the electro-quasistatic formulation is a phasor. Thus, its absolute value and phase are computed to check the validity of the approximate method in comparison to the so-far employed full fidelity method. Aside from this comparison, we in general report the absolute value of the TMP as this is the property of interest in therapeutic applications.

A. 2.5D modeling approach

Firstly, the TMP for the same dielectric parameters as in [17], [23] (see Table I) was computed using the full fidelity as well as the approximate model. The absolute value of the TMP is shown in Fig. 6 along the circular part and in Fig. 7 along the bottom line of the membrane. The TMP is roughly 1.9 times larger along the bottom line than along the circular part for frequencies up to $100\,\mathrm{kHz}$. In this frequency range, the TMP remains constant for both parts. From then on, it starts to change depending on the point on the membrane. Figure 6 shows that at the membrane apex (denoted by the blue line, i.e. an angle of $0°$), the TMP increases from about $1\,\mathrm{MHz}$ to peak at about $10\,\mathrm{MHz}$ before it decreases. A special point on the membrane is the triple point, where membrane, medium and insulator meet. On the circular part, the triple point is located at an angle of $90°$ and on the bottom line, it is located at the cell radius. Close to this point, the TMP drops continuously from about $1\,\mathrm{MHz}$ on and does not peak.

Along the bottom line, it drops for frequencies above $10\,\mathrm{MHz}$ (see Fig. 7). On all points along the bottom line, except the triple point, it it behaves identical. Close to the triple point, it is about $0.1\,\mathrm{mV}$ smaller than at the other points and peaks around $10\,\mathrm{MHz}$ before it drops. Whereas the change along the curved membrane is in the range of a few mV, the drop at the bottom of the membrane is roughly one order of magnitude smaller.

This is in good agreement with previously published results [17]. Note that the electric field other publications focused on can be calculated by dividing the TMP by the membrane thickness. Likewise, the TMP of about $3\,\mathrm{mV}$ corresponds to an electric field strength of $6 \cdot 10^5\,\mathrm{V/m}$ for a membrane of $5\,\mathrm{nm}$ thickness. This result of the axisymmetric 2.5D simulation is about $2 \cdot 10^5\,\mathrm{V/m}$ less than reported for the pure 2D case [17]. Hence, it shows how important the axisymmetric assumption is to account for the real 3D geometry.

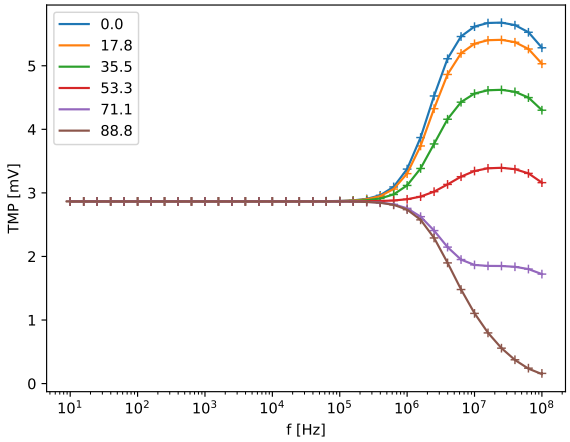

Fig. 6. TMP for a membrane conductivity of $0\,\mathrm{S/m}$ for the 2D model along the circular part. The full fidelity model (solid lines) is compared to the approximate solution at different points on the membrane. The points are characterized by the angle between field and vector from the center of the cell at $(0\,\mu\mathrm{m}, 1\,\mu\mathrm{m})$, i.e. the blue curve corresponds to the cell apex. The relative difference between the two curves is shown in Fig. 8.

1) Accuracy of the approximate method: In all the figures discussed in the preceding paragraph, the full fidelity results were shown together with the approximate results. To access the accuracy of the approximate method in a straightforward manner, we compared the relative error of the result at the different points along the membrane. In that, we compare with the results of the full fidelity as the best possible approximation.

For all points except the triple points, the relative error of the TMP (Figs. 8 and 10) stays below 0.1%. On the bottom line, the relative error is actually only about $10^{-5}\%$ for most of the frequencies (see 10). Close to the triple point, the difference increases and reaches more than 1% on the circular part (Fig. 8) and more than 0.1% on the bottom line (Fig. 10) for high frequencies close to $100\,\mathrm{MHz}$, respectively. In contrast, the phase values are more sensitive towards the method. For small frequencies up to $1\,\mathrm{kHz}$ the results deviate even more

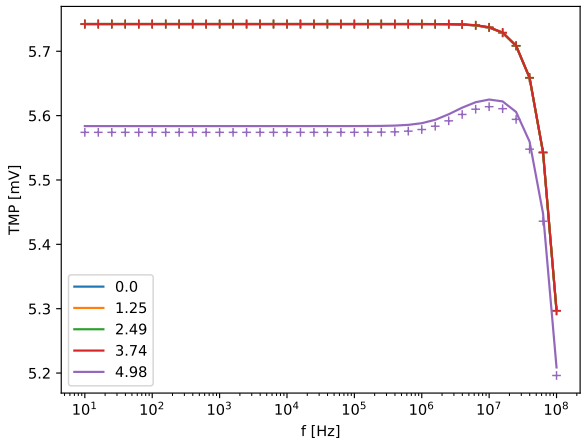

Fig. 7. TMP for a membrane conductivity of $0\,\mathrm{S/m}$ for the 2D model along the bottom line. The full fidelity model (solid lines) is compared to the approximate solution at different points on the membrane. The points are characterized by the distance to the center at $x = 0\,\mu\mathrm{m}$, i.e. all lines except for the point with distance $4.98\,\mu\mathrm{m}$ overlap.

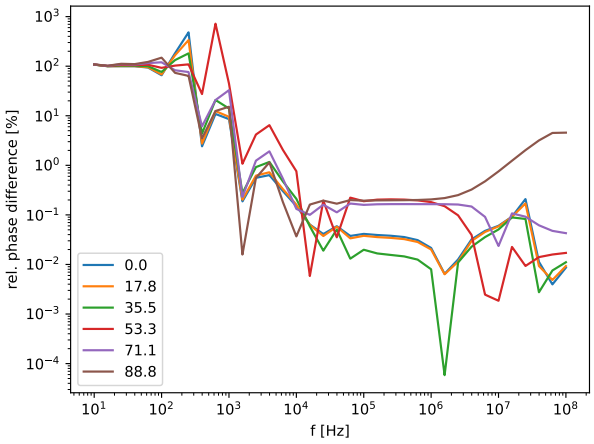

Fig. 9. Relative error of the phase of the TMP along the circular part in case of a membrane conductivity of $0\,\mathrm{S/m}$ for the 2D model in comparison with the full fidelity model.

than 100% (see Figs. 9 and 11). Note that the phase in this frequency region is close to $0°$, and the absolute difference is thus only a few degrees (less than $4°$ for the circular part and less than $4°$ for the bottom line). For larger frequencies, the relative error drops again below 1%.

A possible explanation for the deviations of the phase in the low-frequency range could be a numerical stability problem of the employed direct solver. The ratio between the larger elements and the small elements of the discretized membrane makes the system hard to solve for low frequencies [28]. In COMSOL, this is indicated by a refinement warning. This problem does not occur with the approximate method.

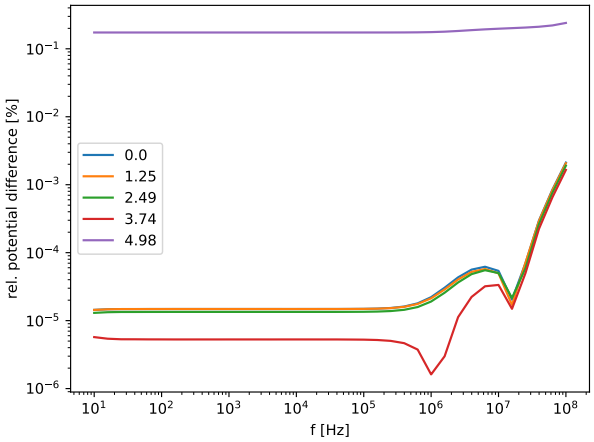

Fig. 10. Relative error of the TMP along the bottom line in case of a membrane conductivity of $0\,\mathrm{S/m}$ for the 2D model in comparison with the full fidelity model as shown in Fig. 7.

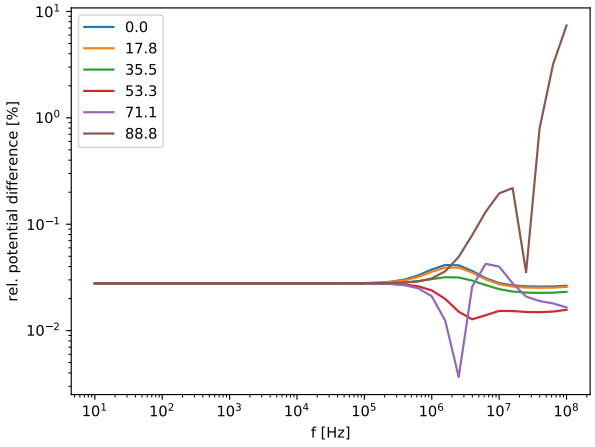

Fig. 8. Relative error of the TMP along the circular part in case of a membrane conductivity of $0\,\mathrm{S/m}$ for the 2D model in comparison with the full fidelity model as shown in Fig. 6.

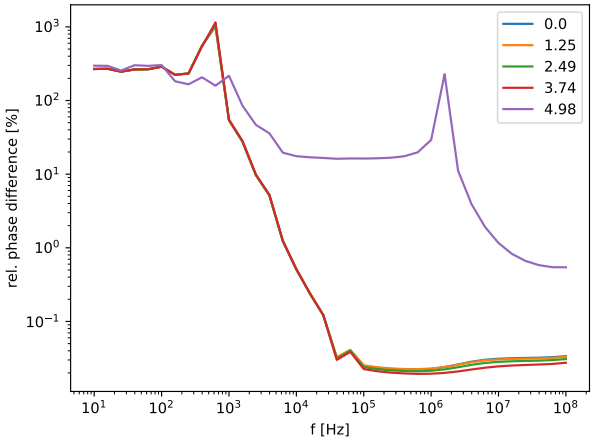

Fig. 11. Relative error of the phase of the TMP along the bottom line in case of a membrane conductivity of $0\,\mathrm{S/m}$ for the 2D model in comparison with the full fidelity model.

2) Parameter dependence: membrane conductivity: There are different model parameters to be investigated. Many of them have been covered in a previous study by Taghian *et*

al. [17]. In this study, we intent to highlight the influence of the membrane conductivity, which has not been studied before. As the membrane is not a perfect insulator, it allows for a leakage current. Realistic values of the membrane conductivity are in the range of $10^{-5}\,\mathrm{S/m}$ to $10^{-8}\,\mathrm{S/m}$ [37]–[39]. We probed conductivities from $0\,\mathrm{S/m}$ (idealized case) to $10^{-3}\,\mathrm{S/m}$ (extreme case, probably perforated membrane). We would like to stress here that the accuracy of the approximate method does not deteriorate if a conductivity greater than $0\,\mathrm{S/m}$ is chosen. Hence, we only report the results of the approximate method in the following. It turns out that changes in the membrane conductivity strongly influence the results (see Figs. 12 and 13, 14 and 15). Upon alteration of the membrane conductivity, a high-pass filter like effect is to be observed.

In contrast to the idealized case of $0\,\mathrm{S/m}$, the TMP is not constant over a broad frequency range. Instead, it is close to zero for low frequencies before it starts to approach the constant value. Nevertheless, this constant value is independent of the conductivity (if the TMP rises at a sufficiently low frequency). The greater the membrane conductivity the higher becomes the frequency, from which on the TMP rises. In the high-frequency limit, the values again coincide irrespective of the membrane conductivity. Speaking in terms of filter, it seems that there exists a 'cut-off frequency' depending on the membrane conductivity. This is also supported by comparisons of the phases (Figs. 14 and 15). A membrane conductivity different to $0\,\mathrm{S/m}$ leads to a phase shift of the TMP that drops only from a certain frequency on.

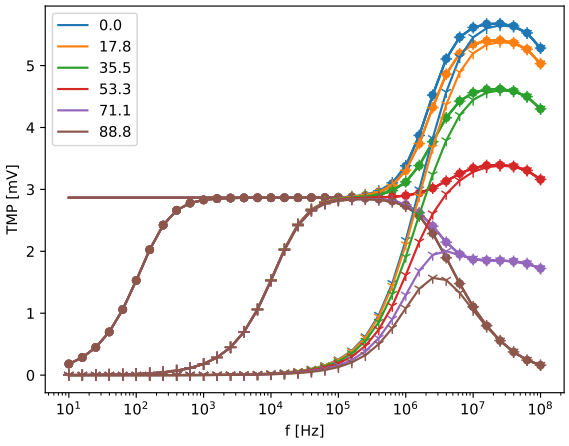

Fig. 12. TMP along the curved part of the cell membrane for different conductivities of $0\,\mathrm{S/m}$ (solid), $1\cdot10^{-7}\,\mathrm{S/m}$ (dots), $1\cdot10^{-5}\,\mathrm{S/m}$ (crosses), $1\cdot10^{-3}\,\mathrm{S/m}$ (triangles). The results were generated using the 'contact impedance' approach.

3) Uncertainty quantification: As the membrane conductivity (compare previous section) and other parameters (compare the findings of [17]) seem to have a significant influence on the modeling result, we chose a mathematically rigorous way to address their influence on the model outcome. Each model parameter can be described by a probability distribution that represents the knowledge about this parameter. It could be a simple estimate as presented in the previous section

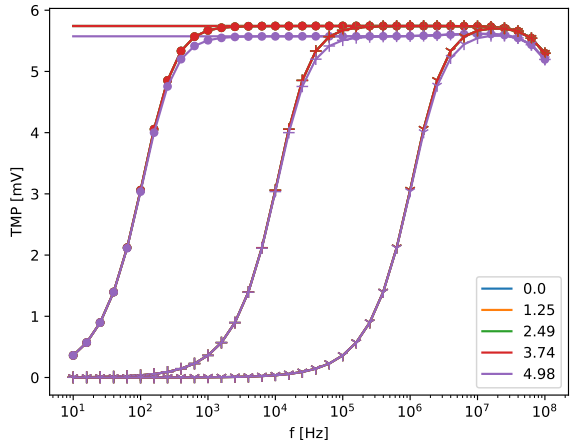

Fig. 13. TMP along the bottom line of the cell membrane for different conductivities of $0\,\mathrm{S/m}$ (solid), $1\cdot10^{-7}\,\mathrm{S/m}$ (dots), $1\cdot10^{-5}\,\mathrm{S/m}$ (crosses), $1\cdot10^{-3}\,\mathrm{S/m}$ (triangles). The results were generated using the 'contact impedance' approach.

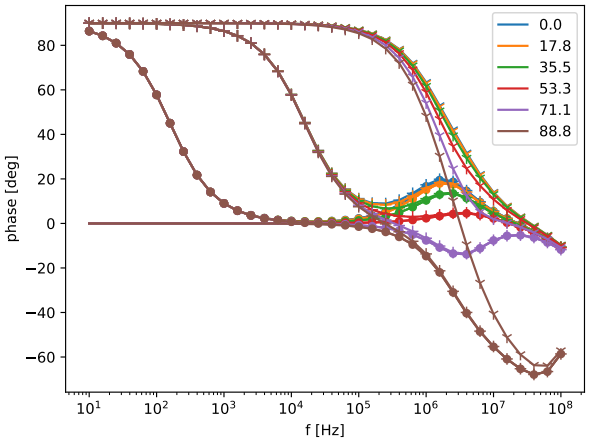

Fig. 14. Phase along the curved part of the cell membrane for different conductivities of $0\,\mathrm{S/m}$ (solid), $1\cdot10^{-7}\,\mathrm{S/m}$ (dots), $1\cdot10^{-5}\,\mathrm{S/m}$ (crosses), $1\cdot10^{-3}\,\mathrm{S/m}$ (triangles). The results were generated using the 'contact impedance' approach.

for the membrane conductivity or a measurement error [40]. To account for the uncertainty, Monte Carlo (MC) sampling methods [41] or the approximate but very efficient Polynomial Chaos (PC) methods [42] can be employed. Recently, the open-source Python package *Uncertainpy* including both methods was published [43]. We utilized a modified version of this package[1] for a PC analysis. We used the default settings of fourth order polynomials (recommended by [44]), point collocation method and 10^4 MC samples to compute the 5^{th} and 95^{th} percentile. The efficiency of the PC methods stems from the fact that a polynomial expansion is used as a surrogate model. The polynomials are chosen with respect to the assumed probability distributions. In a next step, the polynomial expansion coefficients need to be found to construct

[1] https://github.com/j-zimmermann/uncertainpy/tree/1.2.0.1

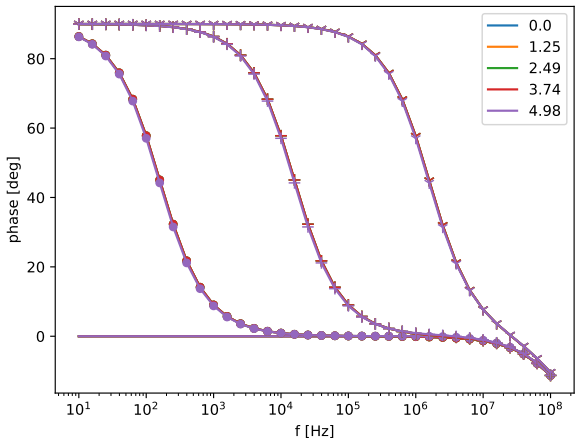

Fig. 15. Phase along the bottom line of the cell membrane for different conductivities of $0\,\mathrm{S/m}$ (solid), $1\cdot10^{-7}\,\mathrm{S/m}$ (dots), $1\cdot10^{-5}\,\mathrm{S/m}$ (crosses), $1\cdot10^{-3}\,\mathrm{S/m}$ (triangles). The results were generated using the 'contact impedance' approach.

the surrogate model. At the collocation points, equality of the model result and the polynomials, i.e. the surrogate model, is enforced. In this sense, *Uncertainpy* generates parameter sets for which the model is evaluated and subsequently computes the polynomial expansion coefficients. The resulting surrogate model is then sampled to obtain the 5^{th} and 95^{th} percentile.

As a first approach, we chose probability distributions relying on sensible assumptions regarding our prior knowledge. These assumptions are summarized in Table II. Since we believe that the parameters of the cell medium and the plastic dish can be measured with high accuracy and thus do not carry a large uncertainty, we focus on the parameters of the cell membrane and the cell cytoplasm. For the cellular parameters, only less accurate methods such as electrorotation, patch clamp or impedance spectroscopy are available [45]. Hence, we propagate the uncertainties of the cellular parameters through the model.

The effect of the parameters' uncertainty is evaluated at the cell apex (i.e., at $0°$) and at the cell bottom (i.e., at $x = 0\,\mu\mathrm{m}$). In total, the model discussed here was run 142 times. The outcome of the UQ analysis is visualized by showing the mean value and the 90% prediction interval of the TMP together with the first-order Sobol indices for each uncertain parameter (see Fig. 16 for the cell apex and Fig. 17 for the cell bottom). In general, Sobol indices serve for variance-based sensitivity analysis. The first-order Sobol indices reveal the individual influence of each parameter on the variance of the TMP value. Higher-order Sobol indices cover the influence due to interactions between the different parameters. The total Sobol indices cover both influences. However, we did not observe a significant difference between first-order and total Sobol indices. Thus, we only report first-order indices. At the cell apex as well as the cell bottom, we observed a prediction interval that is broad in the low-frequency range in comparison to higher frequencies. Nevertheless, in the high-frequency range the prediction interval also becomes broader again at the cell apex. Thanks to the first-order Sobol indices, the variance from the mean can be attributed to the different parameters. In the range up to about $10^3\,\mathrm{Hz}$, the membrane conductivity σ_m plays a crucial role. This was to be expected after the findings presented in Sec. III-A.2. From $10^3\,\mathrm{Hz}$ to $10^6\,\mathrm{Hz}$, the TMP is most sensitive to changes of the membrane permittivity ε_m. For higher frequencies, both membrane permittivity and cytoplasm conductivity σ_cyt contribute with their uncertainty to changes of the TMP at the cell apex. In contrast, the cytoplasm conductivity does not seem to influence the TMP at the cell bottom at higher frequencies (see Fig. 17). Further, the cytoplasm permittivity ε_cyt does not have any influence over the entire frequency range. Its 90% prediction interval is not broader than a few mV for all frequencies.

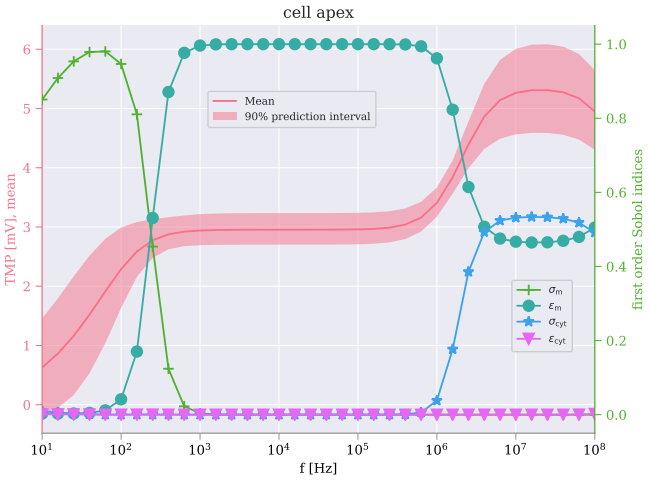

Fig. 16. Left axis: Mean and $\mathbf{90\%}$ prediction interval of the absolute value of the TMP at the cell apex for the abstract model described in Sec. III-A. Right axis: First order Sobol indices for each uncertain parameter, i.e. conductivity (light green) and permittivity (dark green) of the membrane and the conductivity (blue) and permittivity (purple) of the cytoplasm, respectively.

B. Perspectives of the presented approach

In the previous section, we presented the abstract model for a cell and showed, how a rigorous UQ approach can lead to a better understanding of the model outcome and its sensitivities. In this section, we want to discuss the UQ study under more realistic assumptions and comment on the usage of the approximate 'contact impedance' method for 3D applications.

1) UQ based on experimental data: Capacitive coupling is among others used for the electrical stimulation of cartilage [12], bone [46] and their respective cells (osteoblasts [47] and chondrocytes [19], [33]). Since experimental values for the dielectric parameters of chondrocytes are available [39], we focused on chondrocytes. We took the reported values and errors for membrane conductivity, membrane permittivity and cytoplasm conductivity of the PC5 cell line together with the reported average cell radius of $4.1\,\mu\mathrm{m}$ to study the effect of capacitive coupling for the set-up reported in [17]. Furthermore, we applied a membrane thickness of $7\,\mathrm{nm}$ to be

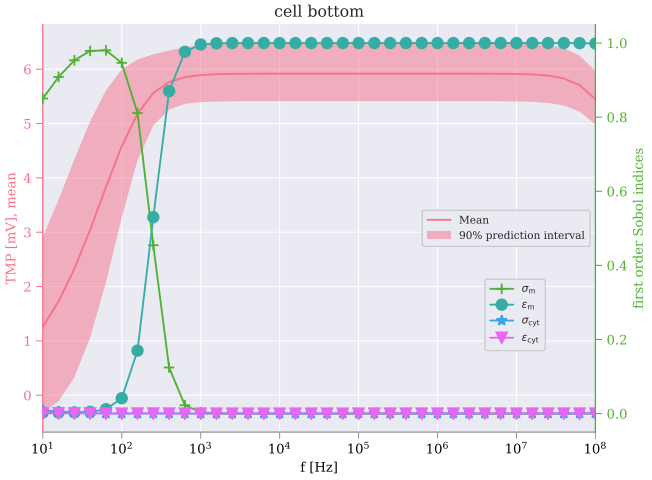

Fig. 17. Left axis: Mean and 90% prediction interval of the absolute value of the TMP at the cell bottom for the abstract model described in Sec. III-A. Right axis: First order Sobol indices for each uncertain parameter, i.e. conductivity (light green) and permittivity (dark green) of the membrane and the conductivity (blue) and permittivity (purple) of the cytoplasm, respectively.

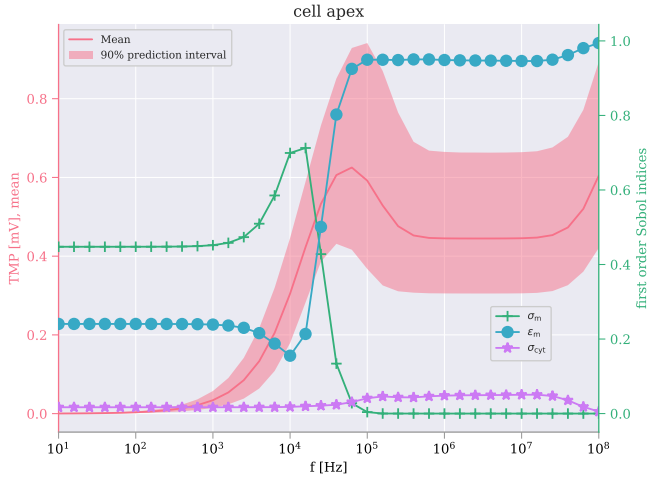

Fig. 18. Left axis: Mean and 90% prediction interval of the absolute value of the TMP at the cell apex for the abstract model described in Sec. III-B.1. Right axis: First order Sobol indices for each uncertain parameter, i.e. conductivity (light green) and permittivity (dark green) of the membrane and the conductivity (blue) and permittivity (purple) of the cytoplasm, respectively.

consistent with [39]. The assumed probability distributions are summarized in Table III. Note that the relatively large conductivity is supported by other experimental findings reporting a large permeability of the chondrocyte membrane for certain ions at rest [48], [49].

This time, we excluded the cytoplasm permittivity as it did not seem to have any influence on the model result. Moreover, it has been set to a fixed value in the original study [39]. As a result, only 72 model realizations are needed for the UQ analysis.

The results are shown in Figs. 18 and 19. Again, the uncertain parameters have an effect on the TMP value. The membrane conductivity plays a dominant role in the low-frequency range, whereas the membrane permittivity influences the results most in the high-frequency range. Interestingly, the comparatively small error of the cytoplasm conductivity also leads to a decreased influence of this parameter. Furthermore, the prediction interval becomes broader for high frequencies in the case studied here. Generally, the TMP value is smaller than in the previous abstract configuration. However, it is still in the mV range that is assumed to have a biological effect [20]. The maximal effect on cell apex as well as bottom can be expected at around $100\,\mathrm{kHz}$.

2) 3D modeling: As not all geometries that are used in the *in vitro* context are axisymmetric, we evaluated if the presented 'contact impedance' approach is also feasible for 3D geometries. For this, we translated the 2D model described in [17] to a 3D model and compared to the 2.5D model described in Sec. III-A. The final model had $4{,}575{,}090$ DOFs, which is more than 100 times more than in the 2D case. The comparison showed good agreement between the two models with deviations of a few percent or less (not shown) or a very small absolute error. Only close to the triple point, the results deviated notably. In our future studies, we intend to use 3D models premised on geometries extracted from *in vitro* experiments via computer-graphics based geometries for the numerical cell models.

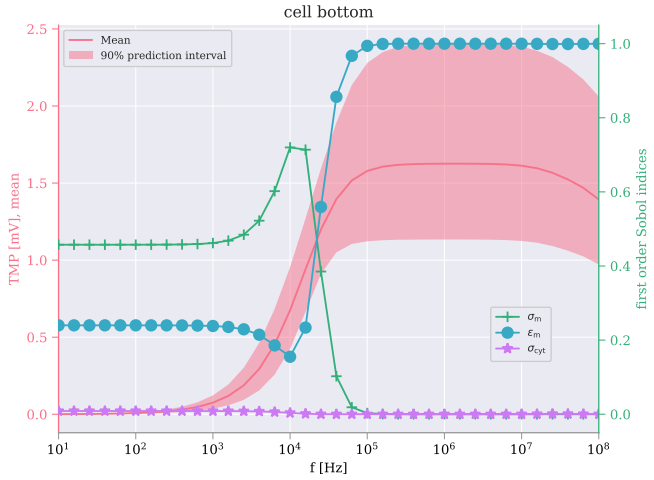

Fig. 19. Left axis: Mean and 90% prediction interval of the absolute value of the TMP at the cell bottom for the abstract model described in Sec. III-B.1. Right axis: First order Sobol indices for each uncertain parameter, i.e. conductivity (light green) and permittivity (dark green) of the membrane and the conductivity (blue) and permittivity (purple) of the cytoplasm, respectively.

TABLE II

PARAMETERS FOR THE UQ STUDY OF THE NUMERICAL MODEL AS REPORTED IN [17], [23]. $\mathcal{U}$ STANDS FOR UNIFORM DISTRIBUTION.

Domain	Quantity	Value	explanation
Cytoplasm	conductivity rel. permittivity	$\mathcal{U}(1, 1.5)[\mathrm{S/m}]$ $\mathcal{U}(60, 80)$	guess assumptions from [39] and [17]
Cell membrane	conductivity rel. permittivity	$\mathcal{U}(0, 10^{-7})[\mathrm{S/m}]$ $\mathcal{U}(9.9, 12.1)$	possible range 10% variation

TABLE III

PARAMETERS FOR THE UQ STUDY OF THE NUMERICAL MODEL AS REPORTED IN [17], [23] APPLIED ON CHONDROCYTES (VALUES BASED ON [39]). $\mathcal{N}$ STANDS FOR NORMAL DISTRIBUTION. NOTE THAT THE CYTOPLASM PERMITTIVITY WAS KEPT FIXED IN THE ANALYSIS IN [39]

Domain	Quantity	Value
Cytoplasm	conductivity	$\mathcal{N}(0.12, 0.02)[\mathrm{S/m}]$
	rel. permittivity	60
Cell membrane	conductivity	$\mathcal{N}(6.895 \cdot 10^{-5}, 1.77 \cdot 10^{-5})[\mathrm{S/m}]$
	rel. permittivity	$\mathcal{N}(59.06, 12.88)$

TABLE IV

COMPUTATIONAL COST FOR DIFFERENT MODELS

Model	DOFs	Solution time in s
Full fidelity 2D	1,390,530	9 min12 s
Contact Impedance 2D	31,713	17 s
Contact Impedance 3D	4,575,090	41 min35 s

IV. DISCUSSION

As shown in Sec. III-A.1, the approximate 'contact impedance' method allows one to keep the accuracy of the numerical model while significantly increasing the computational efficiency. It is a reliable alternative to the full-fidelity membrane model. It even paves the way for simulations of realistic 3D geometries.

Moreover, the approximate method reduces the computational cost such, that a sensitivity analysis of the model by UQ techniques becomes easily feasible (see also Table IV for a comparison of the computational cost). UQ techniques require frequent repetition of the simulation run to sample the parameter space. Nevertheless, the total runtime of the UQ study with the approximate model eventually was of the same order as the runtime of the full-fidelity model.

From the model sensitivities, new information about the system under investigation can be derived. We could show that membrane conductivity and permittivity strongly influence the TMP value depending on the specific frequency range. A membrane conductivity greater than zero introduces a cut-off effect. Below a certain frequency, the TMP of the cell is not changed and remains zero. Only from the cut-off frequency on, the TMP assumes a value that could be physiologically relevant. Thus, we speculate that the electrical stimulation should not be effective below the cut-off frequency. Indeed, studies are often in quest of the appropriate frequency for a stimulation protocol [5], [33], [47]. Our approach could facilitate the choice of the right frequency. We found that for a cell membrane conductivity of up to $10^{-7}\,\mathrm{S/m}$, the stimulation frequency should be above $1\,\mathrm{kHz}$. For chondrocytes, which are a target of capacitively-coupled electrical stimulation [5], [12], [32], [33], a frequency above $10\,\mathrm{kHz}$ but not exceeding $100\,\mathrm{kHz}$ could be most efficient. This conclusion is in good agreement with the experimental findings by [5] that led to the establishment of $60\,\mathrm{kHz}$ as the stimulation frequency in capacitively-coupled stimulation of chondrocytes [33]. Furthermore, a decrease of the TMP with increased membrane conductivity could be found experimentally for DC stimulation [50]. The membrane permittivity does not contribute to the cut-off effect. It only leads to changes of the TMP value. As we could show by comparing two assumptions for the parameter uncertainties, the results of the UQ analysis heavily depend on the *a priori* knowledge of the uncertainties and their distributions.

Still, the presented model is very abstract and does not apply in every case as it neglects the interaction between different cells. Nevertheless, similar models are commonly used across different communities [17], [23], [24], [51]. More sophisticated models including many cells require large high-performance-computing facilities [52]. For types of tissue such as cartilage, where the volume fraction of the cells is small such that the distance between the cells is rather large [53], [54], models including few or only one cell might be sufficient.

V. CONCLUSION

Electrical stimulation is a promising therapeutic tool in regenerative medicine. In *in vitro* experiments, the reaction of individual cell cultures to external electric fields can be studied before translating the gained knowledge to the tissue level. However, to date mostly trial-and-error dominates the experimental approaches. Here, we presented one of the few numerical models in this field of research thus attempting to shed light on the underlying mechanisms of interaction. We focused on capacitive coupling as it has several benefits. By introducing an alternative approximate model for an already established simulation model, we were able to reduce the computational cost significantly without compromising the accuracy. Subsequently, we performed an efficient sensitivity study regarding dielectric cell properties and their individual influence. Our results enable enhanced experimental designs.

In future research, we will advance efficient UQ techniques to enable fast UQ studies for 3D geometries. In that we will transfer knowledge from our previous UQ study on a human brain model [55] to the field of *in vitro* electrical stimulation and promote this UQ approach enabling other researchers to reuse our solution that is based on the open-source tool *Uncertainpy*. A possible application could be in the *TTField* community, where similar cell models are used [51]. Following the research presented in [29]–[31], we will realize an open-source solution for the FEM model.

To enable theoretical multiphysics models, experimental studies on the mechanisms of interaction are needed. A great contribution would be to clarify whether voltage-gated [19] or rather other channels are involved in the signal transduction. This could lead to multiphysics models including, for example, ion dynamics [56] or the mechanical behavior of the membrane [57], [58].

ACKNOWLEDGMENT

Funded by the Deutsche Forschungsgemeinschaft (DFG, German Research Foundation) SFB 1270/1 - 299150580. The authors would like to thank Hendrikje Raben for her support in setting up the Python-MATLAB-COMSOL interface and Konstantin Butenko for making us aware of *Uncertainpy*.

REFERENCES

[1] C. A. L. Bassett and R. J. Pawluk, "Effects of electric currents on bone in vivo," *Nature*, vol. 204, pp. 652–654, 1964.

[2] C. T. Brighton, J. Black, Z. Friedenberg, J. Esterhai, L. Day, and J. Connolly, "A multicenter study of the treatment of non-union with constant direct current." *J Bone Joint Surg Am*, vol. 63, no. 1, pp. 2–13, 1981.

[3] T. Shigino, M. Ochi, H. Kagami, K. Sakaguchi, and O. Nakade, "Application of capacitively coupled electric field enhances periimplant osteogenesis in the dog mandible." *International Journal of Prosthodontics*, vol. 13, no. 5, 2000.

[4] W. Mittelmeier, S. Lehner, W. Kraus, H. P. Matter, L. Gerdesmeyer, and E. Steinhauser, "Biss: concept and biomechanical investigations of a new screw system for electromagnetically induced internal osteostimulation," *Archives of Orthopaedic and Trauma Surgery*, vol. 124, no. 2, pp. 86–91, 2004.

[5] W. Wang, Z. Wang, G. Zhang, C. C. Clark, and C. T. Brighton, "Up-regulation of chondrocyte matrix genes and products by electric fields," *Clin. Orthop. Relat. Res.*, no. 427 SUPPL., 2004.

[6] C. Lee, S. Grad, M. Wimmer, and M. Alini, "The influence of mechanical stimuli on articular cartilage tissue engineering," *Topics in Tissue Engineering*, vol. 2, pp. 1–32, 2006.

[7] J. Xu, W. Wang, C. Clark, and C. Brighton, "Signal transduction in electrically stimulated articular chondrocytes involves translocation of extracellular calcium through voltage-gated channels," *Osteoarthritis and Cartilage*, vol. 17, no. 3, pp. 397–405, 2009.

[8] R. Balint, N. J. Cassidy, and S. H. Cartmell, "Electrical stimulation: A novel tool for tissue engineering," *Tissue Engineering Part B: Reviews*, vol. 19, no. 1, pp. 48–57, Feb 2013.

[9] H. Jahr, C. Matta, and A. Mobasheri, "Physicochemical and biomechanical stimuli in cell-based articular cartilage repair," *Current rheumatology reports*, vol. 17, no. 3, pp. 1–12, 2015.

[10] G. Thrivikraman, S. K. Boda, and B. Basu, "Unraveling the mechanistic effects of electric field stimulation towards directing stem cell fate and function: A tissue engineering perspective," *Biomaterials*, vol. 150, pp. 60–86, Jan 2018.

[11] C. Chen, X. Bai, Y. Ding, and I. S. Lee, "Electrical stimulation as a novel tool for regulating cell behavior in tissue engineering," *Biomater. Res.*, vol. 23, no. 1, pp. 1–12, 2019.

[12] T. Brighton, W. Wang, and C. C. Clark, "The effect of electrical eields on gene and protein expression in human osteoarthritic cartilage expiants," *Journal of Bone and Joint Surgery*, vol. 90, no. 4, pp. 833–848, 2008.

[13] S. Mobini, L. Leppik, V. Thottakkattumana Parameswaran, and J. H. Barker, "In vitro effect of direct current electrical stimulation on rat mesenchymal stem cells," *PeerJ*, vol. 5, p. e2821, Jan 2017.

[14] T. J. Dauben, J. Ziebart, T. Bender, S. Zaatreh, B. Kreikemeyer, and R. Bader, "A novel in vitro system for comparative analyses of bone cells and bacteria under electrical stimulation," *BioMed Research International*, vol. 2016, pp. 1–12, 2016.

[15] D. G. Lorich, C. T. Brighton, R. Gupta, J. R. Corsetti, S. E. Levine, I. D. Gelb, R. Seldes, and S. R. Pollack, "Biochemical pathway mediating the response of bone cells to capacitive coupling," *Clin. Orthop. Relat. Res.*, no. 350, pp. 246–256, 1998.

[16] I. V. Timoshkin, S. J. MacGregor, R. A. Fouracre, B. H. Crichton, and J. G. Anderson, "Transient electrical field across cellular membranes: Pulsed electric field treatment of microbial cells," *J. Phys. D. Appl. Phys.*, vol. 39, no. 3, pp. 596–603, 2006.

[17] T. Taghian, D. A. Narmoneva, and A. B. Kogan, "Modulation of cell function by electric field: a high-resolution analysis," *J. R. Soc. Interface*, vol. 12, no. 107, pp. 20 150 153–20 150 153, 2015.

[18] M. L. Pall, "Electromagnetic fields act via activation of voltage-gated calcium channels to produce beneficial or adverse effects," *J. Cell. Mol. Med.*, vol. 17, no. 8, pp. 958–965, 2013.

[19] J. Xu, W. Wang, C. C. Clark, and C. T. Brighton, "Signal transduction in electrically stimulated articular chondrocytes involves translocation of extracellular calcium through voltage-gated channels," *Osteoarthr. Cartil.*, vol. 17, no. 3, pp. 397–405, 2009.

[20] E. C. Fear and M. A. Stuchly, "Biological cells with gap junctions in low-frequency electric fields," *IEEE Trans. Biomed. Eng.*, vol. 45, no. 7, pp. 856–866, 1998.

[21] M. R. Cho, H. S. Thatte, M. T. Silvia, and D. E. Golan, "Transmembrane calcium influx induced by ac electric fields," *FASEB J.*, vol. 13, no. 6, pp. 677–683, 1999.

[22] K. Budde, J. Zimmermann, E. Neuhaus, M. Schroder, A. M. Uhrmacher, and U. van Rienen, "Requirements for Documenting Electrical Cell Stimulation Experiments for Replicability and Numerical Modeling," in *2019 41st Annu. Int. Conf. IEEE Eng. Med. Biol. Soc.*, 2019, pp. 1082–1088.

[23] J. F. Escobar, J. J. Vaca-González, and D. A. Garzón-Alvarado, "Effect of magnetic and electric fields on plasma membrane of single cells : A computational approach," *Eng. Reports*, vol. e12125, no. September 2019, pp. 1–14, 2020.

[24] G. Pucihar, T. Kotnik, B. Valič, and D. Miklavčič, "Numerical determination of transmembrane voltage induced on irregularly shaped cells," *Ann. Biomed. Eng.*, vol. 34, no. 4, pp. 642–652, 2006.

[25] T. Murovec, D. C. Sweeney, E. Latouche, R. V. Davalos, and C. Brosseau, "Modeling of Transmembrane Potential in Realistic Multicellular Structures before Electroporation," *Biophysical Journal*, vol. 111, no. 10, pp. 2286–2295, 2016. [Online]. Available: http://dx.doi.org/10.1016/j.bpj.2016.10.005

[26] U. van Rienen, J. Flehr, U. Schreiber, S. Schulze, U. Gimsa, W. Baumann, D. G. Weiss, J. Gimsa, R. Benecke, and H. W. Pau, "Electroquasistatic simulations in bio-systems engineering and medical engineering," *Adv. Radio Sci.*, vol. 3, pp. 39–49, 2005.

[27] H. A. Haus and J. R. Melcher, *Electromagnetic fields and energy*. Prentice Hall Englewood Cliffs, NJ, 1989, vol. 107.

[28] I. Meny, N. Burais, F. Buret, and L. Nicolas, "Finite-element modeling of cell exposed to harmonic and transient electric fields," *IEEE Trans. Magn.*, vol. 43, no. 4, pp. 1773–1776, 2007.

[29] A. Agudelo-Toro and A. Neef, "Computationally efficient simulation of electrical activity at cell membranes interacting with self-generated and externally imposed electric fields," *J. Neural Eng.*, vol. 10, no. 2, 2013.

[30] A. Tveito, K. H. Jæger, M. Kuchta, K.-A. Mardal, and M. E. Rognes, "A Cell-Based Framework for Numerical Modeling of Electrical Conduction in Cardiac Tissue," *Front. Phys.*, vol. 5, no. October, pp. 1–18, 2017.

[31] A. J. Ellingsrud, A. Solbrå, G. T. Einevoll, G. Halnes, and M. E. Rognes, "Finite element simulation of ionicelectrodiffusion in cellular geometries," pp. 1–25, 2019. [Online]. Available: http://arxiv.org/abs/1911.03211

[32] J. J. Vaca-González, J. M. Guevara, J. F. Vega, and D. A. Garzón-Alvarado, "An In Vitro Chondrocyte Electrical Stimulation Framework: A Methodology to Calculate Electric Fields and Modulate Proliferation, Cell Death and Glycosaminoglycan Synthesis," *Cell. Mol. Bioeng.*, vol. 9, no. 1, pp. 116–126, 2016.

[33] S. Krueger, S. Achilles, J. Zimmermann, T. Tischer, R. Bader, and A. Jonitz-Heincke, "Re-Differentiation Capacity of Human Chondrocytes in Vitro Following Electrical Stimulation with Capacitively Coupled Fields," *J. Clin. Med.*, vol. 8, no. 11, p. 1771, 2019.

[34] C. T. Brighton, W. Wang, and C. C. Clark, "Up-regulation of matrix in bovine articular cartilage explants by electric fields," *Biochem. Biophys. Res. Commun.*, vol. 342, no. 2, pp. 556–561, 2006.

[35] [Online]. Available: https://github.com/j-zimmermann

[36] [Online]. Available: https://www.comsol.com/blogs/analyze-thin-structures-using-up-and-down-operators/

[37] T. Kotnik, F. Bobanović, and D. Miklavčič, "Sensitivity of transmembrane voltage induced by applied electric fields - A theoretical analysis," *Bioelectrochemistry Bioenerg.*, vol. 43, no. 2, pp. 285–291, 1997.

[38] I. Ermolina, Y. Polevaya, and Y. Feldman, "Analysis of dielectric spectra of eukaryotic cells by computer modeling," *Eur. Biophys. J.*, vol. 29, no. 2, pp. 141–145, 2000.

[39] M. W. Stacey, A. C. Sabuncu, and A. Beskok, "Dielectric characterization of costal cartilage chondrocytes," *Biochim. Biophys. Acta - Gen. Subj.*, vol. 1840, no. 1, pp. 146–152, 2014.

[40] C. J. Roy and W. L. Oberkampf, "A comprehensive framework for verification, validation, and uncertainty quantification in scientific computing," *Comput. Methods Appl. Mech. Eng.*, vol. 200, no. 25-28, pp. 2131–2144, 2011.

[41] C. Lemieux, *Monte Carlo and Quasi-Monte Carlo Sampling*, ser. Springer Series in Statistics. Dordrecht: Springer, 2009.

[42] D. Xiu, *Numerical Methods for Stochastic Computations: A Spectral Method Approach*. USA: Princeton University Press, 2010.

[43] S. Tennøe, G. Halnes, and G. T. Einevoll, "Uncertainpy: A Python Toolbox for Uncertainty Quantification and Sensitivity Analysis in Computational Neuroscience," *Front. Neuroinform.*, vol. 12, no. August, pp. 1–29, 2018.

[44] V. G. Eck, W. P. Donders, J. Sturdy, J. Feinberg, T. Delhaas, L. R. Hellevik, and W. Huberts, "A guide to uncertainty quantification and sensitivity analysis for cardiovascular applications," *Int. J. Numer. Method. Biomed. Eng.*, vol. 32, no. 8, 2016.

[45] Y. Zheng, J. Nguyen, Y. Wei, and Y. Sun, "Recent advances in microfluidic techniques for single-cell biophysical characterization," *Lab Chip*, vol. 13, no. 13, pp. 2464–2483, 2013.

[46] E. L. Carter, E. J. Vresilovic, S. R. Pollack, and C. T. Brighton, "Field distribution in vertebral bodies of the rat during electrical stimulation: a parameter study," *IEEE Transactions on Biomedical Engineering*, vol. 36, no. 3, pp. 333–345, March 1989.

[47] C. C. Clark, W. Wang, and C. T. Brighton, "Up-regulation of expression of selected genes in human bone cells with specific capacitively coupled electric fields," *J. Orthop. Res.*, vol. 32, no. 7, pp. 894–903, 2014.

[48] K. Funabashi, M. Fujii, H. Yamamura, S. Ohya, and Y. Imaizumi, "Contribution of chloride channel conductance to the regulation of resting membrane potential in chondrocytes," *J. Pharmacol. Sci.*, vol. 113, no. 1, pp. 94–99, 2010.

[49] R. Lewis, K. E. Asplin, G. Bruce, C. Dart, A. Mobasheri, and R. Barrett-Jolley, "The role of the membrane potential in chondrocyte volume regulation," *J. Cell. Physiol.*, vol. 226, no. 11, pp. 2979–2986, 2011.

[50] Z. Lojewska, D. L. Farkas, B. Ehrenberg, and L. M. Loew, "Analysis of the effect of medium and membrane conductance on the amplitude and kinetics of membrane potentials induced by externally applied electric fields," *Biophys. J.*, vol. 56, no. 1, pp. 121–128, 1989.

[51] C. Wenger, P. C. Miranda, R. Salvador, A. Thielscher, Z. Bomzon, M. Giladi, M. M. Mrugala, and A. R. Korshoej, "A Review on Tumor-Treating Fields (TTFields): Clinical Implications Inferred from Computational Modeling," *IEEE Rev. Biomed. Eng.*, vol. 11, pp. 195–207, 2018.

[52] P. Mistani, A. Guittet, C. Poignard, and F. Gibou, "A parallel Voronoi-based approach for mesoscale simulations of cell aggregate electropermeabilization," *J. Comput. Phys.*, vol. 380, pp. 48–64, 2019.

[53] J. A. Mollenhauer, "Perspectives on articular cartilage biology and osteoarthritis," *Injury*, vol. 39, no. 1 SUPPL., pp. 5–12, 2008.

[54] M. B. Nagarajan, P. Coan, M. B. Huber, P. C. Diemoz, C. Glaser, and A. Wismuller, "Computer-aided diagnosis in phase contrast imaging x-ray computed tomography for quantitative characterization of ex vivo human patellar cartilage," *IEEE Trans. Biomed. Eng.*, vol. 60, no. 10, pp. 2896–2903, 2013.

[55] C. Schmidt, P. Grant, M. Lowery, and U. Van Rienen, "Influence of uncertainties in the material properties of brain tissue on the probabilistic volume of tissue activated," *IEEE Trans. Biomed. Eng.*, vol. 60, no. 5, pp. 1378–1387, 2013.

[56] C. Poignard, A. Silve, F. Campion, L. M. Mir, O. Saut, and L. Schwartz, "Ion fluxes, transmembrane potential, and osmotic stabilization: A new dynamic electrophysiological model for eukaryotic cells," *Eur. Biophys. J.*, vol. 40, no. 3, pp. 235–246, 2011.

[57] M. Casciola and M. Tarek, "A molecular insight into the electro-transfer of small molecules through electropores driven by electric fields," *Biochimica et Biophysica Acta - Biomembranes*, vol. 1858, no. 10, pp. 2278–2289, 2016. [Online]. Available: http://dx.doi.org/10.1016/j.bbamem.2016.03.022

[58] D. Shamoon, S. Lasquellec, and C. Brosseau, "Perspective: Towards understanding the multiscale description of cells and tissues by electromechanobiology," *Journal of Applied Physics*, vol. 123, no. 24, 2018. [Online]. Available: http://dx.doi.org/10.1063/1.5018723